Monthly Notices of the ROYAL ASTRONOMICAL SOCIETY

MNRAS **504,** 5806–5812 (2021) doi:10.1093/mnras/stab1174
Advance Access publication 2021 May 27

Impact of surface heterogeneity on IR line profiles of adsorbed carbon monoxide on models of interstellar grain surfaces

S. Taj, A. Rosu-Finsen† and M. R. S. McCoustra ★

Institute of Chemical Sciences,Heriot-Watt University, Edinburgh, EH14 4AS, United Kingdom

Accepted 2021 April 20. Received 2021 April 16; in original form 2021 February 18

ABSTRACT

Surface heterogeneity of model amorphous silica films used as a model for interstellar grain surfaces is revealed through the application of the pre-exponential optimized inversion method to previously reported sub-monolayer thermal desorption studies of carbon monoxide (CO) desorption. The impact of that surface heterogeneity, as represented by the coverage dependence of the CO activation energy for desorption from the amorphous silica surface, on the IR spectroscopy of the CO stretching vibration is explored through vibrational line profile synthesis. Comparison is then made to previous investigations of CO line profiles on this surface and on amorphous solid water as reported in Taj et al. (2017, 2019a). A tentative conclusion is drawn that CO vibrationally promoted desorption from, and diffusion on, the amorphous silica surface may be responsible for the correspondingly short vibrational excited state lifetime of CO on that surface. The contrast with CO on amorphous solid water, where direct and rapid vibrational relaxation into the solid water phonon bath occurs, is highlighted. The consequences of this from the standpoint of CO deposition on grain surfaces are discussed.

Key words: astrochemistry – molecular processes – solid state: refractory – solid state: volatile.

1 INTRODUCTION

Solid carbon monoxide (CO) is second most abundant species found in astrophysical ices after water ice. CO ice is readily detected in the infrared through the C–O stretching vibration at around 4.67 μm. Three peaks are frequently evident in this spectral window – two relatively narrow features around 4.674 and 4.665 μm and a broader component around 4.681 μm. The first is usually attributed to CO in an 'apolar' environment, i.e. an environment where weak van der Waals interactions dominate, as in a pure CO ice. The small feature at 4.665 μm is ascribed to either mixtures of solid CO and CO_2 (Boogert, Blake & Tielens 2002; van Broekhuizen et al. 2006) or crystalline CO ice (Pontoppidan et al. 2003a). The broad feature (Tielens et al. 1991; Chiar et al. 1995; Pontoppidan et al. 2003b) is generally attributed to CO in a hydrogen-bonding environment (Sandford et al. 1988; Allamandola et al. 1999). However, observational studies suggest that the hydrogen-bonding environment is likely to be methanol (CH_3OH) instead of water (Cuppen et al. 2011; Penteado et al. 2015), where the CH_3OH is formed through the hydrogenation of CO (Hiraoka et al. 2002; Watanabe et al. 2004; Fuchs et al. 2009; Minissale et al. 2016).

As illustrated by these few examples, it is clear that CO is a very sensitive environmental probe whose utility extends far beyond our Earth-bound laboratories in remotely probing both the gas phase and the solid state in astrophysical environments. Both vibrational frequencies and line profiles demonstrate that environmental sensitivity. Vibrational frequencies shift. These shifts reflect: (i) changes in force fields resulting from intermolecular interaction-induced changes in electron density distributions; and (ii) changes in inertial properties due to geometric changes around vibrational chromophores. Over the years, many empirical correlations have been established reflecting the impact of environment on vibrations for both chromophores in isolated molecules and in molecular clusters. We ourselves have previously published such a correlation for CO on surfaces of relevance to astrophysical environments (Collings, Dever & McCoustra 2014).

Vibrational line profiles are also environmentally sensitive. For isolated molecules, vibrational line profiles are typically symmetric Lorentzian in nature (Atkins & Friedman 2005). In the gas phase, temperature (Doppler Broadening) and pressure (Pressure Broadening) homogeneously broaden of line profiles. With the result that Gaussian or Voigt line profiles are observed (Demtröder 1982). On solid surfaces, molecular translation and rotation are restricted and physisorbed species on simple ionic solids can therefore exhibit relatively narrow linewidths. The work of Ewing and coworkers (Chang, Noda & Ewing 1990; Chang, Dai & Ewing 1995) is a classic example of this. These authors estimate the natural linewidth for the vibration of CO on the NaCl(100) surface at 5 K to be of the order of 10^{-8} cm^{-1} and suggest that the observed linewidth, 0.07 cm^{-1}, results from the residual heterogeneity of the NaCl surface (Chang et al. 1990, 1995). On metal surfaces, oscillating molecular dipoles couple with free electrons in the metal band structure, which provides a fast and efficient mechanism for relaxing excited adsorbate vibrations *via* electron–hole pair creation (Ueba 1997; Arnold 2011). The resulting line profiles are broad, typically ranging from around 5 to 15 cm^{-1} for CO on metal single-crystal surfaces, and asymmetric, reflecting

★ E-mail: M.R.S.McCoustra@hw.ac.uk
† Current Address: Department of Chemistry, University College London, 20 Gordon Street, London, WC1H 0AJ.

Fano coupling between the adsorbate vibration and the non-adiabatic electron–hole pair continuum of the substrate (Gadzuk & Luntz 1984; Langreth 1985). Additionally, these systems, as with halide surfaces, are often subject to further broadening due to environmental heterogeneity (Ryberg 1985). Environmental heterogeneity reaches its extreme with the profiles of vibrational lines of adsorbates interacting with supported metal and metal oxide catalysts (Ryczkowski 2001).

Using the correlation data in Collings et al. (2014), we have explored the origin of CO vibrational line profiles on amorphous silica ($aSiO_2$) and porous amorphous solid water (c-ASW) surfaces using a simple line synthesis methodology (Taj et al. 2017, 2019). This work was based around knowledge of the distribution of binding energies for CO on these surfaces recovered from inversion analysis of the corresponding temperature-programmed desorption data (Collings et al. 2015; Smith, May & Kay 2016). Unfortunately, our earlier work on CO on $aSiO_2$ assumed a fixed pre-exponential factor derived from the work of Redhead (1962) of 1.0×10^{12} s^{-1}, reflecting the physisorption nature of the interaction. In contrast, Smith et al. optimized the pre-exponential factor in their work on the c-ASW surface, obtaining a value of 3.5×10^{16} s^{-1}. In this paper, we therefore present an updated analysis of our previously published temperature programmed desorption (TPD) data for CO desorbing from an $aSiO_2$ surface using the inversion method of Smith et al. (2016) and new simulations on the impact of that heterogeneity on the CO vibrational line profile. This may be of particular relevance, given that Pontoppidan et al. (2003a) tentatively identify CO directly bound to silicate surfaces in some cold, dense environments.

2 RESULTS AND DISCUSSION

The original experiments were described in detail in Taj et al. (2017, 2019) and in the thesis of Taj (2019). Readers are directed to those works and to earlier works describing our experimental apparatus such as Fraser, Collings & McCoustra (2002), Thrower et al. (2009a, 2009b) and Frankland et al. (2015).

At low exposures, the TPD data for CO desorbing from $aSiO_2$ exhibit coincident trailing edges, and as the exposure is increased, a common leading edge is observed (Taj et al. 2017, 2019; Taj 2019). The latter is consistent with multilayer desorption. Identification of the transition between these two distinct behaviours allows us to identify the monolayer (ML) exposure for the $aSiO_2$ surface. This is estimated as 2.88×10^{15} molecules cm^{-2}. Hence, we can define the CO surface coverage in ML for all exposures. Moreover, as there is no evidence to suggest that CO dissociates on $aSiO_2$ at these cryogenic temperatures, we conclude that the coincidence in trailing edges at sub-ML coverages is consistent with the $aSiO_2$ surface presenting a range of binding sites with different binding energies for adsorption, i.e. the surface is heterogeneous, and reflecting the influence of repulsive intermolecular interactions. Additionally, the CO molecules are mobile enough on the $aSiO_2$ surface at these cryogenic temperatures to fill the surface from the most strongly bound to more weakly bound sites with increasing coverage. The mobility of the CO on the $aSiO_2$ surface is something that we will return to consider in interpreting our spectroscopic observations.

Since the assumption of a single value for the activation energy of desorption, $E_{\rm des}$, is no longer valid, direct inversion of the first-order Polanyi–Wigner equation (1) (Attard & Barnes 1998), which defines the rate of desorption, $r_{\rm des}$:

$$r_{\rm des} = \frac{{\rm d}n_{\rm ads}}{{\rm d}t} = \nu\,(n_{\rm ads})\,n_{\rm ads} e^{-\frac{E_{\rm des}}{RT}} \qquad (1)$$

Table 1. Comparison of the inversion analysis from Taj et al. (2017, 2019) and the pre-exponential optimized inversion applied in this case. In Taj et al. (2017, 2019), the pre-exponential was assumed to take a value of 1.0×10^{12} s^{-1} consistent with a physisorption interaction. In the new analysis, the pre-exponential factor was optimized as explained in the text to a value of $1.74^{+0.75}_{-0.53} \times 10^{21}$ s^{-1}.

CO coverage/ ML	$E_{\rm des}$ ($\pm$ 0.5)/kJ mol^{-1} (Taj et al. 2017, 2019a)	$E_{\rm des}$ ($\pm$ 0.5)/kJ mol^{-1} (This work)
0.2	8.1–9.6	14.5–20.1
0.4	7.6–10.2	13.4–19.0
0.6	7.3–8.9	12.7–17.7
0.8	6.9–9.0	12.1–17.7
1.0	6.2–9.0	10.6–17.8

is necessary. Our recent report on heterogeneity in the binding of CO to astrophysically relevant ices (Taj & McCoustra, 2020) describes in detail how, starting from the measured change in CO partial pressure in our ultrahigh vacuum (UHV) system, i.e. the quadrupole mass spectrometer (QMS) count rate which is proportional to $r_{\rm des}$, we can recover the variation of $E_{\rm des}$ with coverage in the sub-ML regime and simultaneously optimize the pre-exponential factor for desorption using the method of Smith et al. (2016).

Fig. ESI-1 shows the results of the optimization of ν using the global sum of residuals squared comparing the observed data with the simulated, χ^2. Table 1 compares the output of our previous inversion analysis with that using the method of Smith et al. (2016), which yields an optimized ν value of $1.74^{+0.75}_{-0.53} \times 10^{21}$ s^{-1}. This value is significantly larger than either normally expected for physisorption (1.0×10^{12} s^{-1}) or for chemisorption (of 1.0×10^{13} s^{-1}) and should be compared to the value of 3.50×10^{16} s^{-1} reported for CO desorbing from amorphous solid water by Smith et al. (2016). It is not unrealistic to assume that the difference in magnitude between these pre-exponential factors recovered by the same method applied to different desorption system reflects differences in the entropy of activation for desorption and hence the entropies of the adsorbed phases as the transition states are likely similar in desorption from amorphous solid water and amorphous silica (Taj, 2019; Taj & McCoustra, 2020).

Why should we undertake this re-analysis? In part, the re-analysis of the data relating to CO desorption from $aSiO_2$ was prompted by making our earlier reports in Taj et al. (2017, 2019) more consistent with our recently reported measurements on astrophysical ices. Of course, if all we were interested in was the rate of CO desorption, as is the case in astrochemical simulations, these could be easily scaled to a new pre-exponential factor. Thus, assuming, we have two interpretations of a sub-ML TPD data set yielding $E_{\rm des,1}(n_{\rm ads})$ and $\nu_1(n_{\rm ads})$, and $E_{\rm des,2}(n_{\rm ads})$ and $\nu_2(n_{\rm ads})$, respectively, it is obvious that since both were derived from the same original rate data using (1), then (2) must hold true with either interpretation being equally valid in describing the desorption kinetics:

$$r_{\rm des} = \nu_1\,(n_{\rm ads})\; e^{-E_{\rm des,1}(n_{\rm ads})/T} = \nu_2\,(n_{\rm ads})\, e^{-E_{\rm des,2}(n_{\rm ads})/T}. \qquad (2)$$

However, the vibrational line profile synthesis does not employ the rate data. Rather, it utilizes the binding energy distribution and that needs to be accurately represented. In assuming the pre-exponential factor, ν, to be 1.0×10^{12} s^{-1}, consistent with a physisorption interaction, for CO desorption from the $aSiO_2$ surface in Taj et al. (2017, 2019), and a value from Smith et al. (2016) for CO desorption from the c-ASW surface, we were inconsistent in the accuracy of our binding energy distributions.

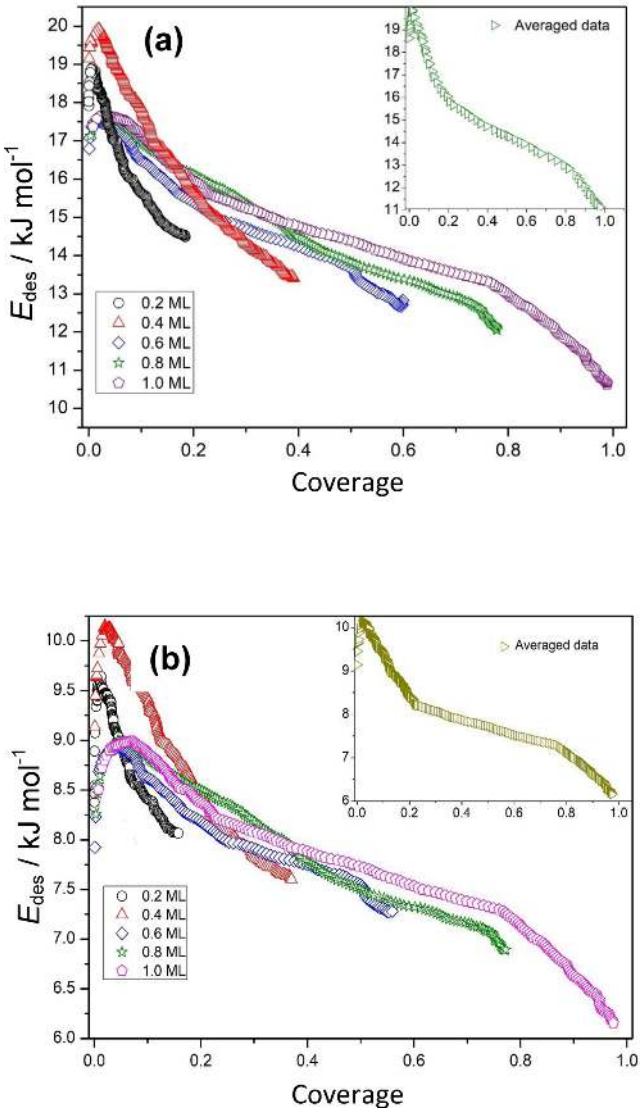

Figure 1. (**a**) E_{des} versus coverage for sub-monolayers of CO desorbing from an $aSiO_2$ substrate derived using ν of $1.74^{+0.75}_{-0.53} \times 10^{21}$ s^{-1} and (**b**) E_{des} versus coverage for sub-monolayers of CO desorbing from an $aSiO_2$ substrate calculated using ν of 1.00×10^{12} s^{-1} as Taj et al. (2017, 2019) and reproduced by permission of the PCCP Owner Societies. The insets contain the averaged data.

Fig. 1 compares the final E_{des} versus coverage data derived from the enhanced inversion analysis with that reported in Taj et al. (2017, 2019). From these data, we can derive the probability distribution of the activation energy for desorption, $P(E_{des})$ versus E_{des}, as given by equation (3):

$$P(E_{des}) = -\frac{dn_{ads}}{dE_{des}} \tag{3}$$

The distribution recovered is shown in Fig. 2 in comparison with that reported in our original work, though it should be noted that subsequent to Taj et al. (2017), we reported a correction to this paper (Taj et al. 2019) and this corrected $P(E_{des})$ distribution from that correction is presented herein. Both distributions are similar to those reported for CO and other small molecules on a number of heterogeneous surfaces. Clearly, the data in Fig. 2 define the range of interaction energies associated with the surface heterogeneity on

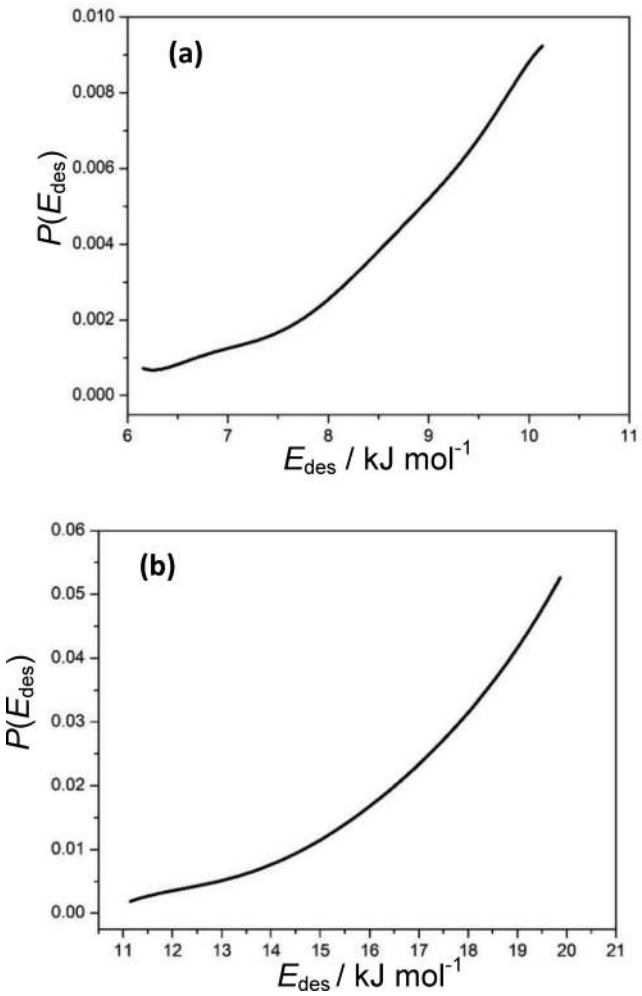

Figure 2. $P(E_{des})$ versus E_{des} as derived from the sub-monolayer TPD of CO from an $aSiO_2$ substrate (**a**) using pre-exponential factor of 1.00×10^{12} s^{-1} from Taj et al. (2017, 2019) and reproduced by permission of the PCCP Owner Societies; (**b**) using the optimized pre-exponential factor of $1.74^{+0.75}_{-0.53} \times 10^{21}$ s^{-1}.

the $aSiO_2$ surface. However, it also gives us the weighting factor associated with each of those energies, i.e. the probability that a CO molecule landing randomly on the $aSiO_2$ surface will find itself in such an environment. Fig. 2 is thus central to the simulation of the CO vibrational line profile in this heterogeneous environment.

The line profile synthesis itself is a relatively simple process as outlined in the sequence described in detail in Taj et al. (2017). To summarize, the correlation of CO vibrational wavenumber frequency shifts $\Delta\overline{\upsilon}(E_{des})$ with interaction energy (equivalent to E_{des}) of Collings et al. (2014) [Taj et al. 2017, equation (6)] was used to yield the distribution of observable wavenumber for the CO vibration on the surface using equation (7) of Taj et al. (2017). The deposition mechanism, stick-and-stop (random ballistic deposition without subsequent diffusion) versus land-and-diffuse (where the most strongly bound sites are filled first), was explored through the resulting intensity distributions in equations (8) and (9) of Taj et al. (2017). In the former, a simple Gaussian line profile was assumed at each E_{des} arising from simple thermal broadening. While in the latter, the accessible energies are restricted to only the strongest through the introduction of an inverse Boltzmann weighting. Good reproduction of the experimental line profile is

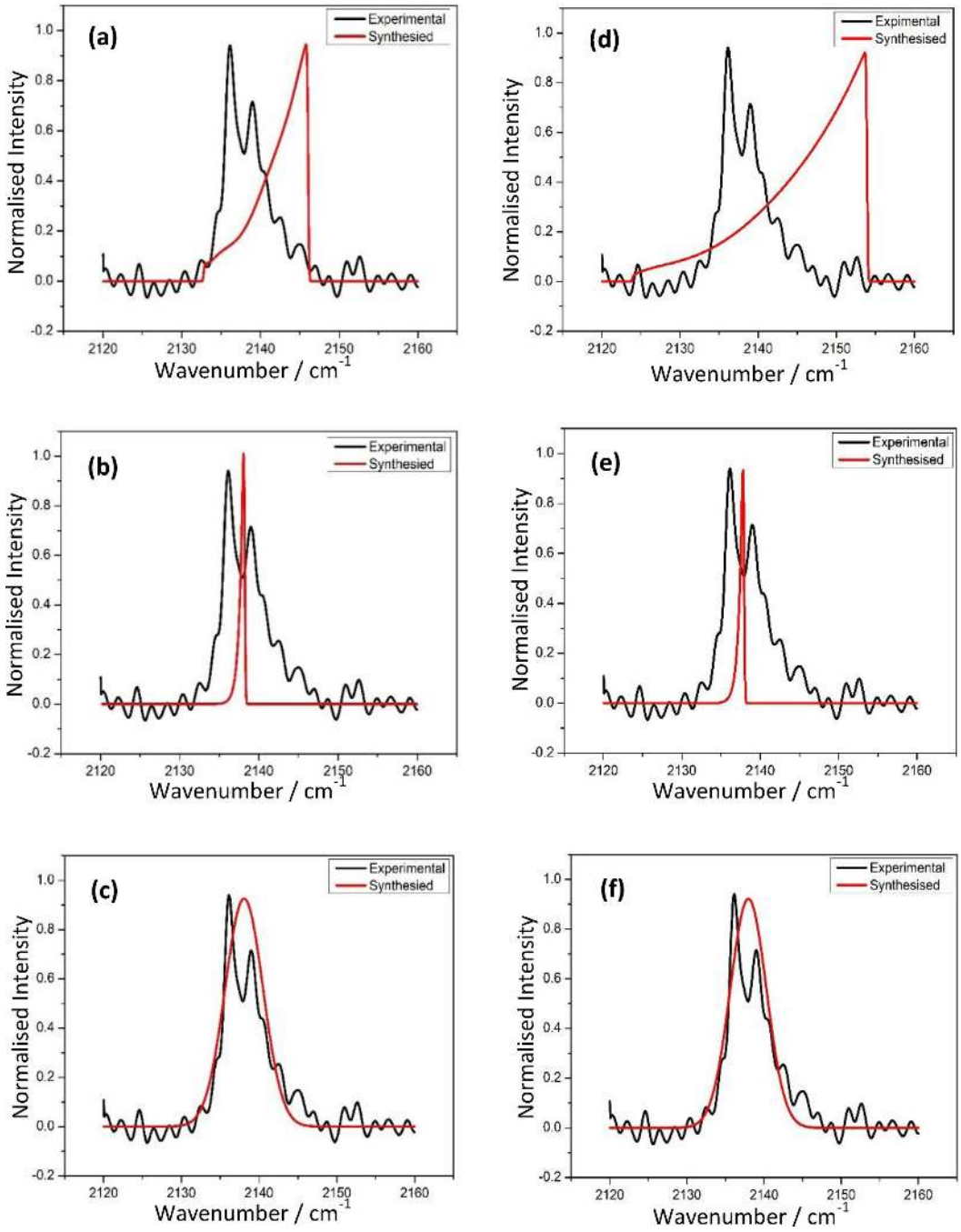

Figure 3. Vibrational line profile synthesis for 0.6 ML CO on $aSiO_2$ assuming (a, d) ballistic deposition and (b, e) adsorb and diffuse deposition at an instrument limited linewidth of 0.1 cm^{-1} while (c, f) show adsorb and diffuse deposition after linewidth optimization. Parts (a)–(c) use the data in Fig. 2a and (d)–(f) from Fig. 2(b).

obtained by variation of three parameters ($\overline{\upsilon}_0$, δ and I_0, – the vibrational wavenumber of CO on a non-interacting surface, the Gaussian linewidth, and the intensity scaling factor) and visual comparison.

Fig. 3 compares the simulated line profiles with the experimental data previously reported in Taj et al. (2017, 2019). Figs 3a and b and Figs 3d and e present simulations made assuming ballistic deposition in **(a)** and **(d)** and adsorb and diffuse mechanism in (b) and (e). The simulations are based on an instrument-limited linewidth of 0.1 cm^{-1} and for the $P(E_{des})$ data in Figs 2a and b, respectively. Neither of these models is consistent with the observed experimental CO IR line profile. It must be concluded that at the deposition temperatures employed in this work of around 15 K, deposition is not ballistic. CO deposition must be occurring through a combination of adsorption and diffusion on the $aSiO_2$ surface, filling the binding sites from the most strongly bound to the least. This is reinforced by Figs 3c and f, where, with the exception of an errant H_2O ro-vibrational feature associated with the optics purge gas, the simulated line profile reproduces the experimental for both $P(E_{des})$ distributions in Fig. 3. The impact of the revised analysis of the line profile synthesis is

summarized in Table 2. The best-fitting full width at half-maximum (FWHM) for the vibrational line profile of CO on $aSiO_2$ is now 5.4 cm^{-1}, which should be compared with the measured FWHM of 5.6 cm^{-1}.

It is clear from the table that the linewidth δ of the CO on $aSiO_2$ line is significantly narrower than for CO on H_2O, 2.4 cm^{-1} versus 3.2 cm^{-1} (Taj et al. 2017, 2019). The revised analysis strengthens this argument in comparing 2.3 cm^{-1} versus 3.2 cm^{-1}. This in turn impacts on the lifetime of the vibrationally excited state of CO, which increases from 1.11 ps corresponding to 2.4 cm^{-1} to 1.15 ps with the revised analysis. This is to compare with 0.83 ps for CO on the H_2O surface.

These lifetimes are exceptionally short. Millikan (1963) reports the gas-phase radiative lifetime of CO to be 33 ms. Measurements on NaCl(100) from Ewing and coworkers (Chang et al. 1990, 1995) suggest a CO radiative lifetime of 0.53 ms on that surface. Both $aSiO_2$ and water are insulators akin to NaCl, so we might expect similar behaviour. In contrast, CO on the semiconducting Si(100) surface exhibits an even shorter vibrational lifetime of around 2.3 ns (Laß, Han & Hasselbrink 2005), which the authors attribute to multiphonon relaxation of the 2081 cm^{-1} CO vibration through an energy coincidence with a multiple of the Si lattice phonon at 520 cm^{-1}. Only on metal surfaces does the vibrational lifetime of CO exhibit ps values (Ueba 1997; Arnold 2011). Could the CO vibration be coupling with the electron–hole pair continuum in the underlying copper substrate? The simple answer to that question is no! Non-adiabatic vibration–electron coupling is readily switched off by the presence of insulating layers (Gadzuk & Luntz 1984; Langreth 1985). This has been experimentally demonstrated to occur for as simple an interposed layer as an ML of a rare gas (Ueba 1997; Arnold 2011), let alone 300 nm of amorphous silica and water ice!

In both systems, CO is likely bound to the substrate via weak hydrogen–bond interactions with the surface OH groups (silanol on $aSiO_2$ and dangling OH from the c-ASW surface). Should we expect the similarity in the estimated vibrational lifetimes to reflect similarities in the potential relaxation pathways of the CO vibration?

Let us begin to answer that question by considering the relaxation of the surface O–H in each system to which the CO is attached. Isolated O–H oscillators on and in solid (Shalit, Perakis & Hamm 2013) and liquid water (Chieffo et al. 2007; Etekhari-Bafrooei & Borguet 2010; Ashihara et al. 2011; Costard et al. 2012; Piatowski et al. 2012; Costard & Elsaesser 2013; Kim, Yeom & Kim 2016; Pastorczak, Nejbauer & Radzewicz 2019) exhibit vibrational lifetimes of around 1–2 ps. The isolated O–H stretching vibrations, including those at surfaces, are strongly coupled to the hydrogen–bond network and hence via the H–O–H bending mode to the low frequency, collective librational modes of bulk H_2O. In the case of CO adsorbed on c-ASW, there is a close energy coincidence between the C–O stretching vibration and the H_2O bending–libration combination band (see Fig. ESI-2). This provides an open gateway for the picosecond time-scale dissipation of the energy in the C–O stretching vibration.

In stark contrast, the vibrational lifetime of the O–H group on silica surfaces has been measured at 200 ps (Heilweil et al. 1989). On the related zeolite surface, the reported lifetime is similar at around 170 ps, which is reduced to around 100 ps with the adsorption of rare gas atoms (Fujino et al. 1996). This lifetime is determined by multiphonon resonant excitation of silica phonon modes by the surface O–H stretching mode akin to the relaxation mechanism of vibrationally excited CO on the Si(100) surface (Laß et al. 2005). A similar mechanism for relaxation of the CO bound to the $aSiO_2$ surface can thus be invoked. However, it is uncertain whether this mechanism would be sufficient to reduce the vibrational lifetime to the observed 2–3 ps as it does not do so on the Si(100) surface!

Are there potential additional mechanisms for reducing the vibrational lifetime of CO adsorbed on $aSiO_2$? The photon energy corresponding to exciting one quantum of the C–O stretch in adsorbed CO on $aSiO_2$ is some 25.6 kJ mol^{-1}. This is significantly in excess of the binding energy range recovered by extended inversion analysis in Table 1. Potentially, vibrational pre-dissociation of the weak CO–silanol bond will provide an additional, or even alternative, mechanism to account for the picosecond CO vibrational lifetime on $aSiO_2$. Vibrational pre-dissociation has long been accepted as an explanation for diffuse spectroscopic behaviour in the IR spectra of gas-phase van der Waals clusters and involves coupling-excited high-frequency intramolecular modes with continuum states in the weak intermolecular mode, which lead to dissociation (Beswick & Jortner 1981; Nesbitt 1994; Bernstein 1995; Nikitin 1999; Yamada, Katsumoto & Ebata 2007; Reisler 2009). The ready availability of ultrafast lasers has even allowed demonstration of vibrational pre-dissociation in condensed-phase media where dissociation of hydrogen bonds is attributed to this mechanism (Graenet et al. 1989; Steinel et al. 2004; Wang, Pang & Dlott 2007; Ottosson, Liu & Bakker 2016). The observed time-scale for these processes is typically several 100 s of femtoseconds to a few picoseconds. Therefore, it is not a significant leap to suggesting that excitation of the C–O stretch of CO weakly hydrogen bonded to silanol entities on the $aSiO_2$ surface will result in vibrational predissociation. This vibrational pre-dissociation may result in desorption of the CO or it may result in enhanced diffusion as desorption and diffusion motions are closely coupled.

3 ASTROPHYSICAL IMPLICATIONS AND CONCLUSIONS

TPD data for CO desorbing from $aSiO_2$ have been re-analysed using an extension to the common inversion analysis method. This analysis produces an optimum value for ν of $1.74^{+0.75}_{-0.53} \times 10^{21}$ s^{-1} and results in much broader range of E_{des} (19.5–11 kJ mol^{-1}) values when compared to using a ν of 1.00×10^{12} s^{-1} (10–6 kJ mol^{-1}) as in the current literature. The distribution of binding energies, $P(E_{des})$, derived in this way was then used to simulate the observed vibrational line profiles of CO adsorbed on both $aSiO_2$ and c-ASW. These simulations confirm that CO is not ballistically deposited under the conditions used in the measurements but undergoes deposition by an 'adsorb and diffuse' mechanism such that the most strongly bound adsorption sites are first populated. They also reveal similar picosecond lifetimes for the CO vibration at what are basically two insulator surfaces.

The near equivalence of the vibrational lifetime of adsorbed CO on $aSiO_2$ and c-ASW surface revealed in this paper is, on detailed consideration, likely to be coincidental.

The water surface promotes very rapid relaxation of excited CO through the energetic coincidence of the bending–libration combination band consistent with the uniquely fast vibrational energy relaxation within water systems. Infrared photodesorption, though energetically feasible, is therefore likely to be inefficient on the c-ASW surface.

The rapid relaxation mechanism available to vibrational excited CO on the c-ASW surface is absent on the $aSiO_2$ surface. Consequently, a combination of multiphonon relaxation and vibrational pre-dissociation is likely to be prevalent on that surface. This means that IR-promoted desorption from or diffusion over the $aSiO_2$ surface is likely to be very much more efficient than on the c-

Table 2. Comparison of the best-fitting parameters, $\bar{\upsilon}_0$ and δ, and of the corresponding FWHM for the modelled and experimental CO vibrational line profiles on $aSiO_2$.

	$\bar{\upsilon}_0$ ($\pm$ 0.5)/cm^{-1}	δ ($\pm$ 0.2)/cm^{-1}	Model FWHM ($\pm$ 0.5)/cm^{-1}	Experiment FWHM ($\pm$ 0.1)/cm^{-1}
CO on $aSiO_2$: Taj et al. (2017); Taj et al. (2019)	2102.5	2.4	5.7	5.6
CO on $aSiO_2$: This work	2069.5	2.3	5.4	5.6

ASW surface. Quantitative comparison of these quantities is clearly required as this could have implications for the time-scale and location of accumulation of CO on icy dust grains, especially where agglomeration of water into clusters is expected to occur in cooling environments (Marchione et al. 2019).

It is clear that vibrational line profiles of CO, in an environmentally heterogeneous surface environment dominated by non-covalent interactions, can be synthesized using a relatively simple, and potentially generalizable, procedure. For such a synthesis, the two main requirements are: (1) knowledge of the impact of the electronic environment on the vibrational frequency or frequencies of the probe molecule under consideration in terms of a correlation as illustrated by the work of Collings et al. (2014); and (2) knowledge of the range of interaction energies and their weighting as encompassed by the $P(E_{\rm des})$ versus $E_{\rm des}$ distribution as illustrated herein. Both of these quantities can, in principle, be derived from high-quality computational chemistry. The challenge in that situation would be in identifying both the size of the system to computationally model and the most cost-effective computational method to apply to that system such that these calculations would accurately reproduce the environmental electronic effects and determine $P(E_{\rm des})$ versus $E_{\rm des}$.

ACKNOWLEDGEMENTS

The authors acknowledge the support of the UK Science and Technology Facilities Council (STFC, ST/M001075/1), the UK Engineering and Physical Sciences Research Council (EPSRC, EP/D506158/1), and the European Community FP7-ITN Marie-Curie Programme (LASSIE project, grant agreement #238258). TS thanks STFC for a project studentship. ARF thanks HWU for a James Watt Scholarship.

DATA AVAILABILITY

The data underlying this article will be shared on reasonable request to the corresponding author.

REFERENCES

Allamandola L. J., Bernstein M. P., Sandford S. A., Walker R.L., 1999, Space Sci. Rev., 90, 219
Arnold H., 2011, Prog. Surf. Sci., 86, 1
Ashihara S., Fujioka S., Shibuya K., 2011, Chem. Phys. Lett., 502, 57
Atkins P., Friedman R., 2005, Molecular Quantum Mechanics, Fourth Edition. Oxford University Press, Oxford, UK, Chapter 6
Attard G., Barnes C., 1998, Surfaces. Oxford University Press. Oxford
Bernstein E. R., 1995, Annu. Rev. Phys. Chem., 46, 197
Beswick J. A., Jortner J., 1981, Adv. Chem. Phys. 47
Boogert A. C. A., Blake G. A., Tielens A. G. G. M., 2002, ApJ, 577, 271
Chang H.-C., Dai D. J., Ewing G.E., 1995, J. Chin. Chem. Soc., 42, 317
Chang H.-C., Noda C., Ewing G. E., 1990, J. Vac. Sci. Technol. A: Vac. Surf. Films, 8, 2644
Chiar J. E., Whittet D. C. B., Kerr T. H., Adamson A. J., 1995, ApJ, 455, 234
Chieffo L., Shattuck J., Amsden J. J., Erramilli S., Ziegler L. D., 2007, Chem. Phys., 341, 71
Collings M. P., Dever J. W., McCoustra M. R. S., 2014, PCCP, 16, 3479
Collings M. P., Frankland V. L., Lasne J., Marchione D., Rosu-Finsen A., McCoustra M. R. S., 2015, Mon. Not. R. Astron. Soc., 449, 1826
Costard R., Elsaesser T., 2013, J. Phys. Chem. B, 117, 15338
Costard R., Levinger N. E., Nibbering E. T. J., Elsaesser T., 2012, J. Phys. Chem. B, 116, 5752
Cuppen H. M., Penteado E. M., Isokoski K., van der Marel N., Linnartz H., 2011, Mon. Not. R. Astron. Soc., 417, 2809
Demtröder W., 1982, Laser Spectroscopy. Springer-Verlag, Heidelberg, Chapter 3
Etekhari-Bafrooei A., Borguet E., 2010, J. Am. Chem. Soc., 132, 3756
Frankland V. L., Rosu-Finsen A., Lasne J., Collings M. P., McCoustra M. R. S., 2015, Rev. Sci. Instrum., 86, 055013
Fraser H. J., Collings M. P., McCoustra M. R. S., 2002, Rev. Sci. Instrum., 73, 2161
Fuchs G. W., Cuppen H. M., Ioppolo S., Romanzin C., Bisschop S. E., Andersson S., van Dishoeck E. F., Linnartz H., 2009, A&A, 505, 629
Fujino T. et al., 1996, J. Chem. Phys., 105, 279
Gadzuk J. W., Luntz A.C., 1984, Surf. Sci., 144, 429
Graener H., Ye T. Q., Laubereau A., 1989, J. Chem. Phys. 91, 1043
Heilweil E. J., Casassa M. P., Cavanagh R. R., Stephenson J.C., 1989, Annu. Rev. Phys. Chem., 40, 143
Hiraoka K., Sato T., Sato S., Sogoshi N., Yokoyama T., Takashima H., Kitagawa S., 2002, ApJ, 577, 265
Kim C., Yeom M. S., Kim E., 2016, Korean J. Chem. Eng., 33, 255
Langreth D. C., 1985, Phys. Rev. Lett., 54, 126
Laß K., Han X., Hasselbrink E., 2005, J. Chem. Phys. 123, 051102
Marchione D. et al., 2019, ACS Earth Space Chem., 3, 1915
Millikan R. C., 1963, J. Chem. Phys., 38, 2855
Minissale M., Moudens A., Baouche S., Chaabouni H., Dulieu F., 2016, Mon. Not. R. Astron. Soc., 458, 2953
Nesbitt D. J., 1994, Annu. Rev. Phys. Chem., 45, 367
Nikitin E. E., 1999, Annu. Rev. Phys. Chem., 50, 1
Ottosson N., Liu L., Bakker H. J., 2016, J. Phys. Chem. B, 120, 7154
Pastorczak M., Nejbauer M., Radzewicz C., 2019, PCCP, 21, 16895
Penteado E. M., Boogert A. C. A., Pontoppidan K. M., Ioppolo S., Blake G. A., Cuppen H. M., 2015, Mon. Not. R. Astron. Soc., 454, 531
Piatkowski L., Wexler A. D., Fuchs E. C., Schoenmaker H., Bakker H. J., 2012, Phys. Chem. Chem. Phys., 14, 6160
Pontoppidan K. M., Fraser H., Schoier F. L., Dartois E., Thi W. F., van Dishoeck E. F., 2003b, in Fich M., eds, Chemistry as a Diagnostic of Star Formation. National Research Council, Ottawa, Canada, p. 390
Pontoppidan K. M. et al., 2003a, A&A, 408, 981
Redhead P. A., 1962, Vacuum, 12, 203
Reisler H., 2009, Annu. Rev. Phys. Chem., 60, 39
Ryberg R., 1985, Phys. Rev. B, 32, 2671
Ryczkowski J., 2001, Catal. Today, 68, 263
Sandford S. A., Allamandola L. J., Tielens A. G. G. M., Valero G. J., 1988, ApJ, 329, 498
Shalit A., Perakis F., Hamm P., 2013, J. Phys. Chem. B, 117, 15512
Smith R. S., May R. A., Kay B. D., 2016, J. Phys. Chem. B, 120, 1979

Steinel T., Asbury J. B., Zheng J. R., Fayer M. D., 2004, J. Phys. Chem. A, 108, 10957
Taj S., 2019, PhD thesis, Heriot-Watt University, Edinburgh, UK
Taj S., Baird D., Rosu-Finsen A., McCoustra M. R. S., 2017, PCCP, 19, 7990
Taj S., Baird D., Rosu-Finsen A., McCoustra M. R. S., 2019, *PCCP*, 21, 21633
Taj S., McCoustra M. R. S., 2020, Mon. Not. R. Astron. Soc., 498, 1693
Thrower J. D., Collings M. P., Rutten F. J. M., McCoustra M. R. S., 2009a, Mon. Not. R. Astron. Soc., 394, 1510
Thrower J. D., Collings M. P., Rutten F. J. M., McCoustra M. R. S., 2009b, J. Chem. Phys., 131, 244711
Tielens A. G. G. M., Tokunaga A. T., Geballe T. R., Baas F., 1991, ApJ, 381, 181
Ueba H., 1997, Prog. Surf. Sci., 55, 115
van Broekhuizen F. A., Groot I. M. N., Fraser H. J., van Dishoeck E. F., Schlemmer S., 2006, A&A, 451, 723
Wang Z., Pang Y. S., Dlott D. D., 2007, J. Phys. Chem. A, 111, 3196
Watanabe N., Nagaoka A., Shiraki T., Kouchi A., 2004, ApJ, 616, 638
Yamada Y., Katsumoto Y., Ebata T., 2007, Phys. Chem. Chem. Phys., 9, 1170

SUPPORTING INFORMATION

Supplementary data are available at *MNRAS* online.

Figure ESI-1: The x^2 between experimental and simulated TPD of CO from aSiO_2 for all initial coverages versus the log of the pre-exponential factor used in the inversion analysis using the method of Smith et al. (2016)
Figure ESI-2: IR spectra of amorphous solid SiO_2 (URL 2019a) and solid H_2O (URL 2019b).

Please note: Oxford University Press are not responsible for the content or functionality of any supporting materials supplied by the authors. Any queries (other than missing material) should be directed to the corresponding author for the article.

This paper has been typeset from a Microsoft Word file prepared by the author.